COMMUNICATION

Scrolled Poly(*L*-lactic acid) Single Crystals via Chain End-Induced Symmetry-Breaking

Shichen Yu,[a] Seyong Kim,[a] Kingsley O. Ojima,[b] Bin Zhao, [b] and Christopher Y. Li* [a]

[a] Shichen Yu, Dr. Seyong Kim, and Prof. Christopher Y. Li
Department of Materials Science and Engineering
Drexel University
Philadelphia, PA 19104, United States
E-mail: chrisli@drexel.edu (CYL)

[b] Kingsley O. Ojima and Prof. Bin Zhao
Department of Chemistry
University of Tennessee
Knoxville, Tennessee 37996, United States

Supporting information for this article is given via a link at the end of the document.

Abstract: Single crystals that do not obey translational symmetry have been reported in various material systems. In polymers, twisted crystals are typically formed in banded spherulites, while a class of non-flat polymer single crystals (PSCs) has been observed. Herein, we report the formation of scrolled single crystals of biodegradable polymer poly(*L*-lactic acid) (PLLA). While classical 2-dimensional single crystals formed in solution-crystallized PLLA are flat, we show that PLLA crystals bend into scrolls in low molar mass PLLA. The formation of these unique scrolled PLLA single crystals depends on polymer chain ends and the polymer molecular weight. This work, therefore, demonstrates a new mechanism to break translational symmetry in PSC growth.

Translational symmetry breaking in crystal growth manifests in many non-flat crystal morphologies observed in small molar mass organic molecules, polymers, and inorganic materials.[1] Intriguing crystalline morphologies such as helicoidal, scrolled, tubular, and spherical crystals are observed.[1-2] Since the translational symmetry is broken, these structures can be considered a class of shape-symmetry incommensurate crystals (SSICs).[3] A typical reason for symmetry breaking in polymeric systems is unbalanced stress on the lamellar surface.[4] For example, classical lamellar twisting in spherulites is attributed to the unbalanced stress associated with chain tilting or the volumetric mismatch of fold surfaces.[5] Chirality on the macromolecular level can be transferred to single crystal and spherulite levels.[6] In thin films, this structural imbalance often leads to the bending of thin lamellae.[7] Two-dimensional (2D) asymmetric crystals can be realized in triblock copolymers and molecular bottlebrushes, and by crystallizing in nanoemulsions.[8]

Scrolled polymer single crystals (PSCs) represent another type of SSICs. Polymer scrolled crystals have been reported in polyamide (PA) and poly(vinylidene fluoride) (PVDF).[9] Scroll/tubular morphologies were observed in solution-grown PA66 PSCs.[9a, 10] The formation of the symmetry-breaking nanoscrolls was attributed to the unbalanced folding from the amine and acid moieties of the polymer chain. In PVDF, Lotz *et al.* proposed that the excess stress created by the volumetric differences in the opposite fold surfaces forces the scrolling of the lamellae.[11] Isolated γ-phase PVDF PSC nanoscrolls were obtained via solution crystallization.[12] Besides PA66 and PVDF, similar scrolled crystals were observed in isotactic poly(1-butene)[13] and centrally substituted alkanes.[14]

Poly(*L*-lactic acid) (PLLA) is a sustainable polymer whose crystallization behaviour in bulk, solution, and thin films has been extensively studied.[15] Typical 2D lamellae have been observed in solution and thin film crystallization, while one-dimensional (1D) fibrillar crystals were recently reported in Langmuir-Blodgett films and from evaporative crystallization on water surfaces.[16] While these crystals differ in morphology, they all obey translational symmetry. Non-flat morphology was seen in PLLA spherulites and PLLA-containing block copolymers.[17] In this work, we report the observation of symmetry-breaking in PLLA PSCs grown in solution. Scrolled PSCs were obtained, and the crystal structure was characterized using wide-angle X-ray diffraction (WAXD) and selected area electron diffraction (SAED). The crystal symmetry breaking was attributed to the end-group-induced unbalanced lamellar surfaces. Our results demonstrate yet another means to introduce symmetry breaking in PSCs.

Table 1 summarizes the chemical structures and molecular characteristics of the polymers used in this study. Size exclusion chromatography (SEC) was used to confirm the molecular weights (MW) of all polymers. PLLA with one end functionalized with *N*-ethylmaleimide and the other end being a hydroxy group ($PLLA_{8.9k}$-MI, number average molar mass M_n = 8.9 kDa, $Đ$ =1.19, and the subscript denotes the M_n) was first used in this study since the large *N*-ethylmaleimide end groups are relatively easy to be excluded from the PLLA crystalline lattice. Using a self-seeding method, $PLLA_{8.9k}$-MI single crystals were grown in 1-hexanol.[18] The self-seeding temperature (T_s) was 110 °C, and the crystallization temperature (T_c) was 80 °C (**Figure S1** is the crystallization temperature profile).

Table 1. Molecular characteristics of the PLLA polymers.

Molecular Structure	Sample	Source[a]	Molar Mass (M_n, g/mol)[b]	Dispersity (Đ)
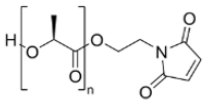	$PLLA_{8.9k}$-MI	Sigma Aldrich	8.9k	1.19
	$PLLA_{15k}$-MI	Our lab	15k	1.11
	$PLLA_{29k}$-MI	Our lab	29k	1.10
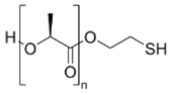	$PLLA_{9.7k}$-SH	Sigma Aldrich	9.7k	1.21
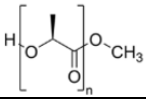	$PLLA_{10k}$-ME	Sigma Aldrich	10k	1.11

[a] $PLLA_{8.9k}$-MI, $PLLA_{9.7k}$-SH, and $PLLA_{10k}$-ME were purchased from Sigma Aldrich. $PLLA_{15k}$-MI and $PLLA_{29k}$-MI were synthesized in our laboratories.
[b] Measured using size exclusion chromatography relative to polystyrene standards.

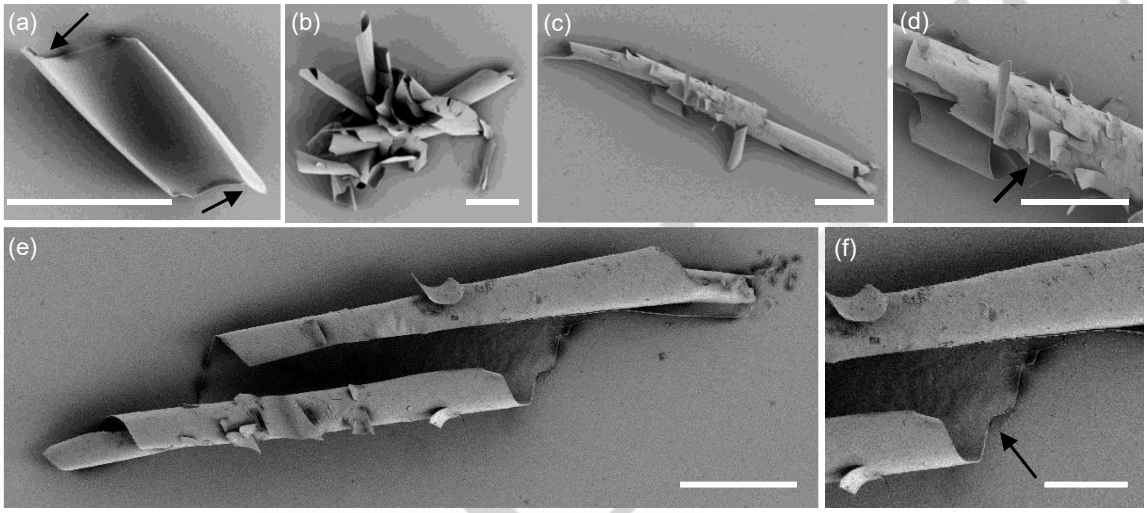

Figure 1. SEM images of $PLLA_{8.9k}$-MI crystals grown from a 0.05 wt.% 1-hexanol solution, T_S = 110 °C, T_c = 80°C. (a) t = 5 min; (b-f) t = 20 min. Scale bars: (a) and (f) 10 μm, (b-e) 20 μm.

Figures 1 and **S2** show the representative crystal morphology. A non-flat crystal is observed after 5 min of crystallization (**Figure 1a**. SEM images of PSCs collected at the crystallization time t = 3 and 10 min are shown in **Figure S2**). The crystal bends along its long axis with off-center tips, indicated by the arrows. The long axis is approximately parallel to the two edges of the crystal. At a longer crystallization time of 20 min, both scroll clusters (Figure 1b) and elongated scroll crystals are seen (Figure 1c-f). The scrolls are relatively long, with a length of ~160 μm and a diameter of 10 μm (Figure 1c), likely due to the continued growth along the crystal's long axis. The enlarged image in **Figure 1d** reveals dense overgrowth and branching from the original tube, which will be discussed later. Some of the scroll crystals appear as pairs (**Figure 1e**. **Figure S3** shows another pair), connected by the underneath lamella (**Figure 1f**), suggesting that they are formed by the bending of a single lamella from the opposite sides. The scrolled morphology confirms that these PLLA crystals are another example of SSICs,[3] as the translational symmetry is broken in the direction transverse to the scroll axis.

The crystal structure of the scrolled crystals was investigated using WAXD and SAED. **Figure S4** depicts the WAXD pattern with the diffraction peaks at 2θ = 14.8°, 17.1°, 18.9°, and 22.4°, assigned as (010), (110)/(200), (203), (015) planes of α form PLLA with an orthorhombic unit cell with *a* = 1.0683 nm, *b* = 0.6170 nm, and *c* = 2.8860 nm.[19] Transmission electron microscopy (TEM) image of a $PLLA_{8.9k}$-MI scrolled crystal and the corresponding SAED are shown in **Figure 2a-c**. The circles in **Figure 2a** indicate the areas where the SAED patterns were collected. Areas 1 and 2 are at the centre and on the edge of the scroll, respectively. As shown in **Figure 2b**, the diffraction pattern from area 1 comprises six diffraction spots characteristic of the [00*l*] zone of α form PLLA, consistent with the simulated pattern in **Figure 2d**. The scroll axis is vertical in **Figure 2a** and perpendicular to the (110) diffraction spots in **Figure 2b**, indicating the scroll axis is parallel to the (110) plane. The diffraction pattern collected from area 2 consists of multiple zones (**Figure 2c**). This is because, near the edge of the scroll, more crystals with different lattice orientations project onto the selected area compared to the centre of the scroll, more likely to produce a multiple zone diffraction pattern. Detailed analysis suggests that these diffraction spots are associated with $(3\bar{1}0)$, $(2\bar{1}1)$, $(1\bar{1}3)$, $(0\bar{1}1)$, $(\bar{1}\bar{1}3)$, $(20\bar{3})$ planes, as indicated in the figure, and these diffractions can be assigned to three different zones: $(0\bar{1}1)$ is from [133] zone(labelled blue); $(2\bar{1}1)$ and $(\bar{1}\bar{1}3)$ are from [273] zone(labelled yellow); and $(1\bar{1}3)$ and $(20\bar{3})$ are from [392] zone(labelled green) (**Figure 2e-g** are the simulated SAED patterns using CrystalMaker®). The diffraction

results confirm that the scrolling axis is along $< 1\bar{1}0 >$, parallel to the (110) plane and perpendicular to the *c* axis. All the three zone axes can be reached by rotating the PLLA crystal in a [00l] zone orientation about the scroll axis, *e.g.*, 14° for [133]; 29° for [273]; and 48° for [392].

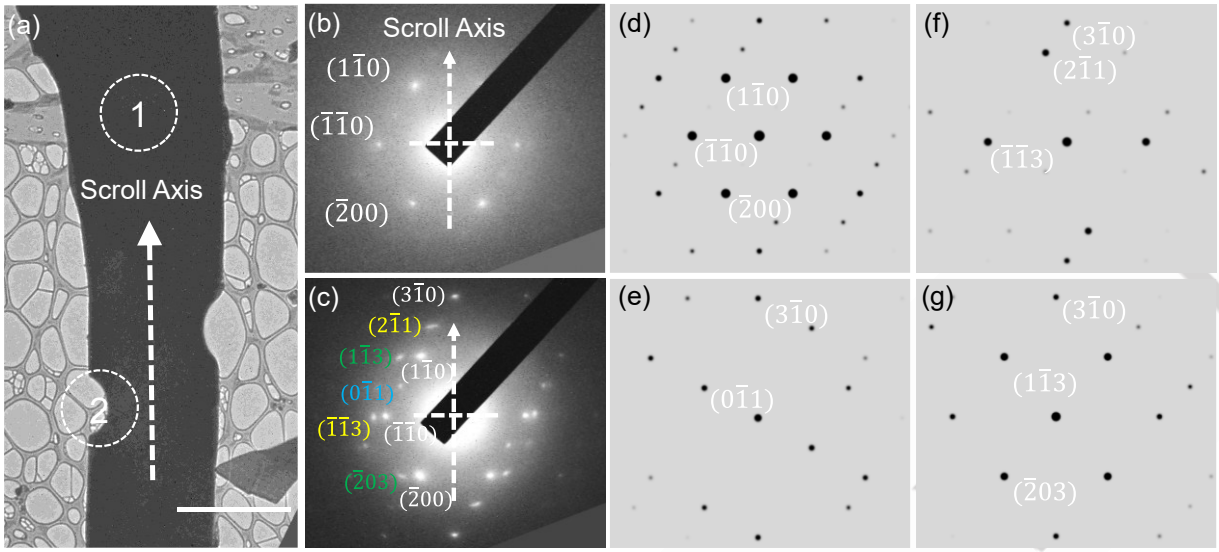

Figure 2. (a) TEM image of a $PLLA_{8.9k}$-MI scroll crystallized at 80 ℃ for 20 min (scale bar: 4 μm). The inset circle indicates the areas where diffraction was collected. (b-c) SAED pattern collected from area 1(b) and area 2 (c). (d-g) Simulated SAED patterns of (d) [00l], (e) [133], (f) [273] and (g) [392] zones.

Why do $PLLA_{8.9k}$-MI crystals bend into a scrolled shape? We hypothesize that the bulky chain ends play an important role in the scroll morphology formation. To this end, methoxy/hydroxy end-terminated PLLA (10 kDa, $PLLA_{10k}$-OMe) and 2-mercaptoethyl-($HSCH_2CH_2$-)/hydroxy end-terminated PLLA (9.7 kDa, $PLLA_{9.7k}$-SH) single crystals were grown using the same condition (**Table 1**). Note that these polymers have similar M_n and $Đ$. $PLLA_{9.7k}$-SH produces scrolled crystals similar to $PLLA_{8.9k}$-MI (**Figure 3a**), while slightly curved crystals are obtained in $PLLA_{10k}$-OMe (**Figure 3b**). The three samples have similar M_n and the same -OH group on one chain end. However, their other chain ends differ. The chain end volume can be estimated by partial volumes of functional groups,[20] yielding 0.146 nm^3 for *N*-ethylmaleimide and 0.100 nm^3 for 2-mercaptoethyl, which are larger than the methoxy end group (0.056 nm^3). They are all larger than the volume of -OH (0.022 nm^3), with the difference between *N*-ethylmaleimide and the hydroxy the greatest, suggesting that the difference in the size of the two chain ends is related to the PSC scrolling.

The crystal thickness was measured using atomic force microscopy (AFM) to illustrate the lamellar scrolling mechanism further. Taking the $HSCH_2CH_2$-ended $PLLA_{9.7k}$-SH as an example, the average thickness of the $PLLA_{9.7k}$-SH lamellae is 11.5 nm (**Figure 3c,** AFM images of $PLLA_{8.9k}$-MI are shown in **Figure S5**.). The number of folds per chain in the lamellae can be estimated by $n_{fold} = \frac{n*l}{h_c} - 1$, where *l* is the projected length of the lactic acid repeating unit onto the chain axis (*l* = 0.2886 nm using the 10_3 helical conformation for the α phase), h_c is the crystal thickness, and *n* is the number of repeating units (135 in this case). The fold number in this scroll crystal is ~ 2.4. The bulky chain ends are anticipated to be excluded to the crystal surfaces, and the surface area density of the $-CH_2CH_2SH$ chain end groups is related to the inverse of the chain fold number, assuming the $-CH_2CH_2SH$ groups evenly distributed on the two sides of the crystal: $\sigma = \frac{1}{2a \times b \times (n_{fold}+1)}$. A high -SH chain end density of 0.22 nm^{-2} is formed on the crystal, which could impose stress on the 2D lamellae. Note that both symmetrical and asymmetrical chain end distributions on the two lamellar surfaces are feasible, as shown in **Figure 3d**. The asymmetrical end group distribution could lead to unbalanced stress and, therefore, lamellar bending.

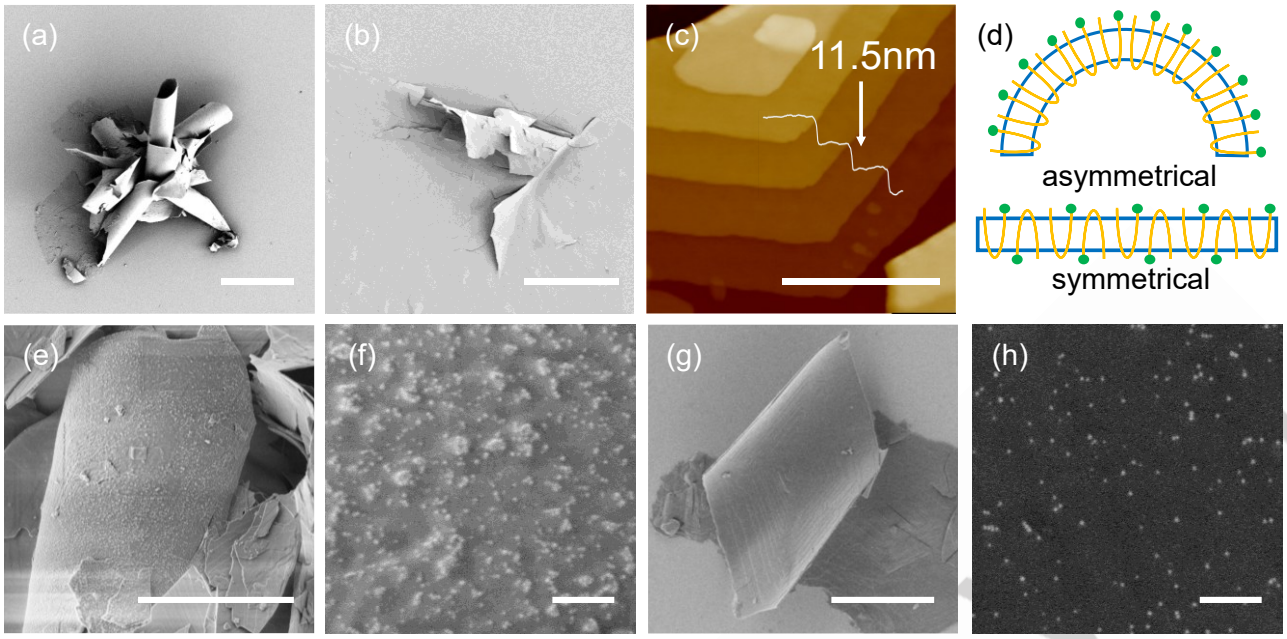

Figure 3. SEM images of single crystals of (a) $PLLA_{9.7k}$-SH and (b) $PLLA_{10k}$-OMe crystallized at 80 ℃ for 20 min. (c) AFM image $PLLA_{9.7k}$-SH crystals obtained by crystallization at 80 ℃ for 3min. (d) Schematic of symmetric and asymmetric distribution of chain ends in a PSC (showing a fold number of 1 as an example). (e-f) Outer surface and (g-h) Inner surfaces of the $PLLA_{9.7k}$-SH scrolled crystal. Scale bars: (a) and (b) 20μm, (e) and (g) 5μm, (C) 1μm, (f) and (h) 100nm.

Nanoparticle decoration was used to confirm the asymmetric chain end distribution in the scroll crystals with $PLLA_{9.7k}$-SH as the model polymer since they form similar scroll crystals as $PLLA_{8.9k}$-MI, and the thiol end group on the PSC surface can bind with gold nanoparticles (AuNPs).[21] The AuNP density can then serve as a marker for the chain end distribution. For ease of imaging, half-opened $PLLA_{9.7k}$ -SH scroll crystals were collected at t = 5 min, and the PSC suspension was mixed with a AuNP colloid. The morphology of AuNP-attached crystals is shown in **Figure 3e-h**. AuNPs were observed on both the inner and outer scroll surfaces. For each side, a 1 x 1 μm area was selected to estimate the AuNP areal density (**Figure S6**). The outer surface has a denser AuNP coating, over 3 times, compared to the inner surface (492 and 150 AuNPs/μm^2, respectively, detailed counting of AuNPs is shown in Figure S6). The significant difference in AuNP number density indicates that the -SH end group density differs between the two surfaces. Since PLLA chains fold approximately 2.4 times in this crystallization condition, approximately 22% of the outer surfaces are occupied by thiol end groups and ~ 7% for the inner surface

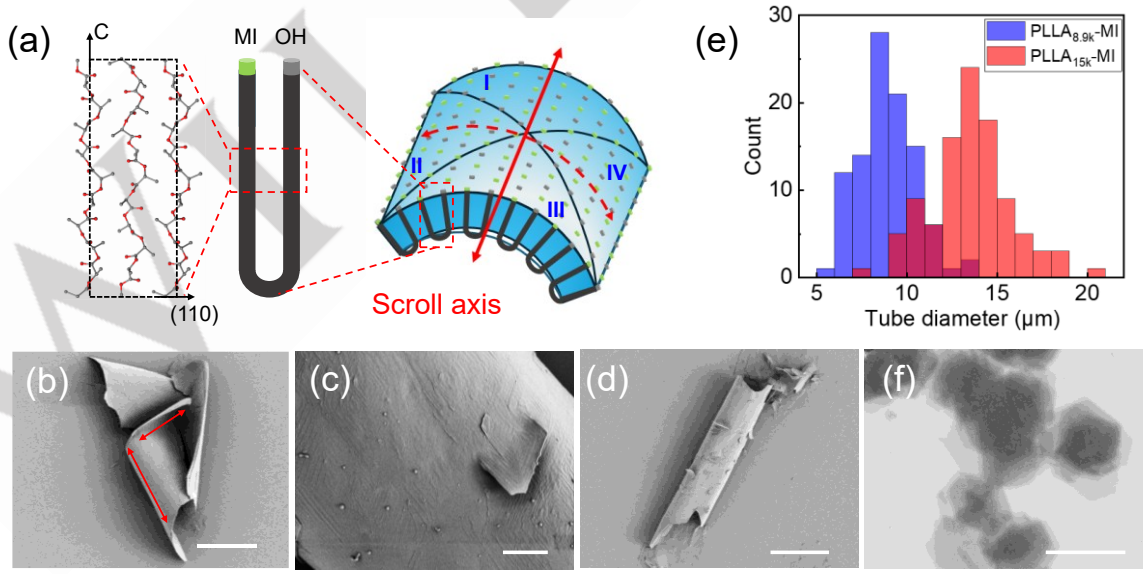

Figure 4. (a) Schematic of a PLLA scroll crystal's hierarchical structure. (b) SEM image of $PLLA_{8.9k}$-MI scrolls. The scrolling direction changes in one PSC. (c) SEM image of the surface of a scrolled crystal, showing the overgrowth and lamella branching. (d) SEM image of $PLLA_{15k}$-MI scroll crystal crystallized at 80 °C. (e) Histogram of the scroll crystal diameter of different MW PLLA-MI crystallized at 80 °CEach distribution is from 100 measurements on acquired SEM images. (f) SEM image of flat crystals formed from $PLLA_{29k}$-MI crystallized at 80 °C. Scale bars: (c) 10μm, (d) 1μm, (e) 20μm, (f) 1μm.

The asymmetric arrangement of the end groups induces unbalanced stress on the lamellar surfaces. To release this stress, the observed scrolled crystal bend along the (110) plane with a scroll axis of $< 1\bar{1}0 >$. The scroll axis is likely determined by the chain fold direction in the PLLA α lamellae. **Figure 4a** shows a schematic representation of a PLLA crystal. The preferred fold direction is {110} planes, suggesting that sheets of crystalline stems connected by folds are formed along the {110} planes, bending orthogonal to this set of planes would likely be easier. Note that in the early stage of the growth, since no crystalline lattice splay is needed along the scroll axis while chains have to deviate from the desired lattice along the orthogonal direction, the growth rate along the scroll axis is greater, generating an anisotropic growth along the scroll axis direction, and the crystal evolves from a "normal" flat lozenge-shaped crystals to an anisotropic crystal shown in **Figure 1a**. Once the two ends of the crystal meet to form the scroll, the lateral growth would be further slowed down due to limited materials access to the growth front.

The {110} planes represent the slowest growing directions and (110) and $(\bar{1}10)$ are 60° to each other in PLLA α crystals. As shown in **Figure 4a**, when the scroll axis is parallel to (110) planes of PSC sectors II and IV, the fold directions in sectors I and III are 60° from the scroll axis. Therefore, in sectors II and IV, the splay of the chains only occurs along layers of (110) planes. However, in sectors I and III, the splay direction is at an acute angle to the folding direction. Since the {110} planes in the four sectors are crystallographically equivalent, a second scroll axis can be developed due to lamellar branching. The frequent changes in the lamellar bending directions, *e.g.* from $(\bar{1}10)$ to (110), can often be observed as shown in **Figures 1c,d,** and highlighted in **Figures 4b,c**. The (110) plane of the overgrown lamellae can be clearly seen in **Figure 4c**. The branching habit, therefore, further confirms the bending orthogonal to {110}, which most effectively alleviates the stress. Note that this is different from the scrolling of PA66 and PVDF, which is related to the fold volume mismatch.[9a, 11]

Varying the polymer MW can further test the asymmetric lamella hypothesis because, with a similar lamellar thickness, a longer chain would lead to a lower end-group areal density on the crystal surface, therefore, less surface stress. **Figure 4d** shows the SEM image of scrolls formed by 15 kDa PLLA-MI ($PLLA_{15k}$-MI). The observed average scroll diameter is 13.6 μm, significantly higher than 8.9 μm in $PLLA_{8.9k}$-MI (**Figure 4e**). The lamellae thicknesses of these crystals are similar to those revealed by the AFM experiments (**Figure S5**). Because of the higher MW, $PLLA_{15k}$-MI chains have to fold more times than $PLLA_{8.9k}$-MI, 4.7-times fold compared to 2.1-times fold. Therefore, the end group surface areal density is decreased, which mitigates the surface end group effects, leading to less unbalanced surface stress and generating scroll crystals with larger diameters. A higher MW 29 kDa PLLA ($PLLA_{29k}$-MI) was used for crystallization to reduce the end-group effect further. Only the classical flat 2D crystals were observed with a similar lamellar thickness of 11.7 nm (**Figures 4f, S6d**), further confirming the end-group effect on the crystal growth.

Conclusion

Solution crystallization of end-functionalized PLLA was conducted to investigate the chain-end effect on PLLA crystallization. Scrolled PSCs were observed in low MW PLLA-MI and PLLA-SH. XRD and SAED confirmed the α form PLLA crystal structure. Detailed analysis showed that the crystal scroll axis is along $< 1\bar{1}0 >$ and parallel to the (110) plane. Chain end distribution analysis by AFM and AuNP decoration revealed the asymmetrical distribution of the chain ends on the 2D crystal surface. This, combined with the relatively large size of the chain ends in PLLA-MI and PLLA-SH, produced unbalanced stress on the two crystal surfaces, leading to lamella scrolling. This unbalanced stress can be relaxed with increasing MW, as evidenced by larger scroll diameter and, eventually, flat crystals seen in PLLA-MI with higher Mw.

Twitter handle: @Chrisyli

Supporting Information

The authors have cited additional references within the Supporting Information.[22]

Acknowledgements

CYL and BZ are grateful for the funding support from NSF (DMR-2104968 and -2412257, respectively). The authors thank Dr. Bernard Lotz for insightful discussions.

Keywords: Chiral crystals • sustainable polymers • polymer single crystals • scrolled crystals • crystal engineering

References

[1] a) W. Wang, H. Qi, T. Zhou, S. Mei, L. Han, T. Higuchi, H. Jinnai, C. Y. Li, *Nat. Commun.* **2016**, *7*, 10599; b) A. Bausch, M. J. Bowick, A. Cacciuto, A. Dinsmore, M. Hsu, D. Nelson, M. Nikolaides, A. Travesset, D. Weitz, *Science* **2003**, *299*, 1716-1718; c) E. Yashima, N. Ousaka, D. Taura, K. Shimomura, T. Ikai, K. Maeda, *Chem. Rev.* **2016**, *116*, 13752-13990; d) W. Ma, L. Xu, A. F. de Moura, X. Wu, H. Kuang, C. Xu, N. A. Kotov, *Chem. Rev.* **2017**, *117*, 8041-8093; e) A. G. Shtukenberg, Y. O. Punin, A. Gujral, B. Kahr, *Angew. Chem. Int. Ed.* **2014**, *53*, 672-699.

[2] a) L. Gao, S. Mei, Q. Qian, S. Yu, B. Zhao, Y. Tu, C. Y. Li, *Angew. Chem. Int. Ed.* **2023**, *62*, e202217267; b) J. Xu, H. Ye, S. Zhang, B. Guo, *Crystals* **2017**, *7*, 241.

[3] M. C. Staub, C. Y. Li, *Polymer* **2020**, 122407.

[4] a) H. Keith, F. Padden, *Macromolecules* **1996**, *29*, 7776-7786; b) B. Lotz, S. Z. D. Cheng, *Polymer* **2005**, *46*, 577-610; c) A. J. Lovinger, *Macromolecules* **2020**, *53*, 741-745.

[5] H. Keith, F. Padden Jr, B. Lotz, J. Wittmann, *Macromolecules* **1989**, *22*, 2230-2238.

[6] a) C. Y. Li, S. Z. D. Cheng, J. J. Ge, F. Bai, J. Z. Zhang, I. K. Mann, F. W. Harris, L. C. Chien, D. H. Yan, T. B. He, B. Lotz, *Phys. Rev. Lett.* **1999**, *83*, 4558-4561; b) C. Y. Li, S. Z. D. Cheng, J. J. Ge, F. Bai, J. Z. Zhang, I. K. Mann, L. C. Chien, F. W. Harris, B. Lotz, *J. Am. Chem. Soc.* **2000**, *122*, 72-79.

[7] D. Maillard, R. E. Prud'homme, *Macromolecules* **2008**, *41*, 1705-1712.

[8] a) H. Qi, X. Liu, D. M. Henn, S. Mei, M. C. Staub, B. Zhao, C. Y. Li, *Nat. Commun.* **2020**, *11*, 2152; b) H. Qi, H. Zhou, Q. Tang, J. Y. Lee, Z. Fan, S. Kim, M. C. Staub, T. Zhou, S. Mei, L. Han, *Nat. Commun.* **2018**, *9*, 3005; c) M. C.

Staub, S. Kim, S. Yu, C. Y. Li, *ACS Macro Lett.* **2022**, *11*, 1022-1027; d) M. C. Staub, S. Yu, C. Y. Li, *Macromol. Rapid Commun.* **2022**, 2200529; e) M. C. Staub, S. Yu, C. Y. Li, *Giant* **2022**, 100124; f) J. T. Wilk, C. T. Furner, E. W. Kent, M. T. Kelly, B. Zhao, C. Y. Li, *Macromolecules* **2024**, *57*, 8487−8497.

[9] a) W. Cai, C. Y. Li, L. Li, B. Lotz, M. Keating, D. Marks, *Adv. Mater.* **2004**, *16*, 600-605; b) A. Vaughan, *J. Mater. Sci.* **1993**, *28*, 1805-1813.

[10] B. Lotz, S. Cheng, C. Li, *Macromolecules* **2018**, *51*, 5138-5156.

[11] B. Lotz, A. Thierry, S. Schneider, *Comptes Rendus de l'Academie des Sciences Series IIC Chemistry* **1998**, *10*, 609-614.

[12] G. R. Burks, H. Qi, S. E. Gleeson, S. Mei, C. Y. Li, *ACS Macro Lett.* **2018**, *7*, 75-79.

[13] T. Wen, H.-J. Sun, B. Lotz, S. Z. Cheng, *Macromolecules* **2020**, *53*, 7570-7579.

[14] H. White, I. Hosier, D. Bassett, *Macromolecules* **2002**, *35*, 6763-6765.

[15] a) S. Saeidlou, M. A. Huneault, H. Li, C. B. Park, *Prog. Polym. Sci.* **2012**, *37*, 1657-1677; b) M. L. Di Lorenzo, R. Androsch, *Synthesis, Structure and Properties of Poly (lactic acid), Vol. 279*, Springer, **2018**.

[16] a) S. Ni, W. Yin, M. K. Ferguson-McPherson, S. K. Satija, J. R. Morris, A. R. Esker, *Langmuir* **2006**, *22*, 5969-5973; b) K. Watanabe, J. Kumaki, *Polym. J.* **2020**, *52*, 601-613; c) C. Fuchs, K. Busse, A. K. Flieger, J. Kressler, *Chemical Engineering & Technology* **2016**, *39*, 1333-1340; d) A. Das, A. S. El-Tawargy, E. Khechine, S. Noack, H. Schlaad, G. n. Reiter, R. Reiter, *Langmuir* **2019**, *35*, 6129-6136; e) A. Das, S. Noack, H. Schlaad, G. n. Reiter, R. Reiter, *Langmuir* **2020**, *36*, 8184-8192; f) Q. Qian, S. Yu, C. Y. Li, *Macromolecules* **2023**; g) Q. Qian, C. T. Furner, C. Y. Li, *Langmuir* **2024**, *40*, 6285-6294.

[17] Y.-W. Chiang, R.-M. Ho, C. Burger, H. Hasegawa, *Soft Matter* **2011**, *7*, 9797-9803.

[18] D. J. Blundell, A. Keller, A. J. Kovacs, *J. Polym. Sci. Polym. Phys.* **1966**, *4*, 481-486.

[19] K. Wasanasuk, K. Tashiro, M. Hanesaka, T. Ohhara, K. Kurihara, R. Kuroki, T. Tamada, T. Ozeki, T. Kanamoto, *Macromolecules* **2011**, *44*, 6441-6452.

[20] R. F. Fedors, *Polymer Engineering & Science* **1974**, *14*, 147-154.

[21] B. Li, C. Y. Li, *J. Am. Chem. Soc.* **2007**, *129*, 12-13.

[22] N. R. Jana, X. Peng, *J. Am. Chem. Soc.* **2003**, *125*, 14280-14281.

Entry for the Table of Contents

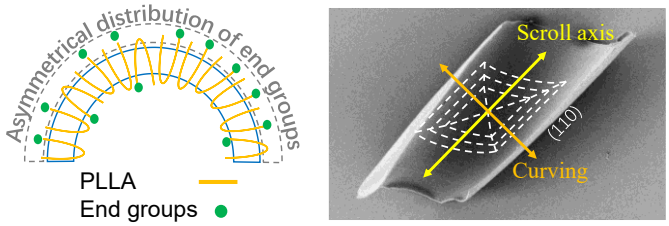

Scrolled single crystals of biodegradable poly(L-lactic acid) with broken translational symmetry were obtained using solution crystallization. The scrolling mechanism was attributed to the imbalance of the fold surfaces arising from the asymmetrical distribution of the polymer chain ends, experimentally confirmed by nanoparticle decoration. This work demonstrates a new strategy for breaking crystal translational symmetry in polymer single crystals.